

RSC Advances



This is an *Accepted Manuscript*, which has been through the Royal Society of Chemistry peer review process and has been accepted for publication.

Accepted Manuscripts are published online shortly after acceptance, before technical editing, formatting and proof reading. Using this free service, authors can make their results available to the community, in citable form, before we publish the edited article. This *Accepted Manuscript* will be replaced by the edited, formatted and paginated article as soon as this is available.

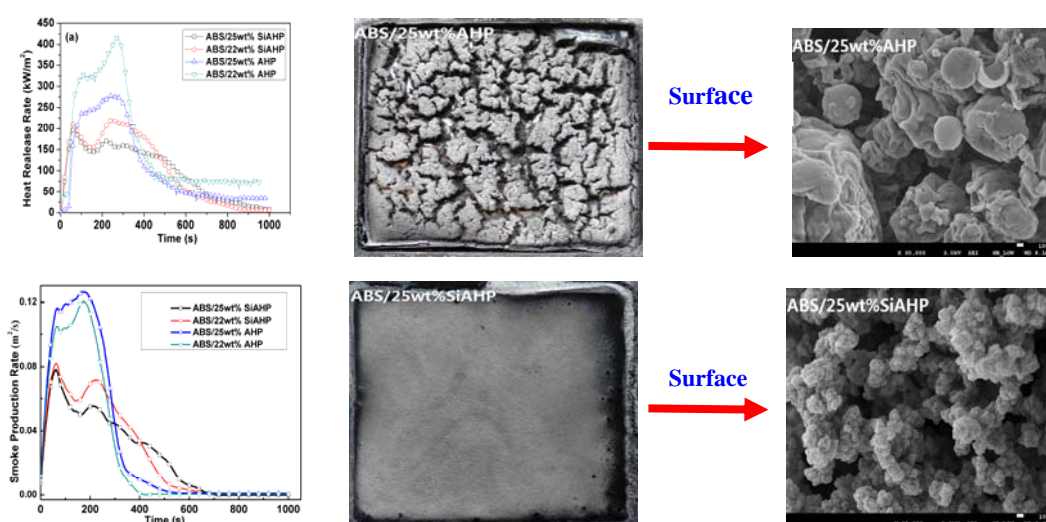
You can find more information about *Accepted Manuscripts* in the [Information for Authors](#).

Please note that technical editing may introduce minor changes to the text and/or graphics, which may alter content. The journal's standard [Terms & Conditions](#) and the [Ethical guidelines](#) still apply. In no event shall the Royal Society of Chemistry be held responsible for any errors or omissions in this *Accepted Manuscript* or any consequences arising from the use of any information it contains.

Surface Microencapsulation Modification of Aluminum Hypophosphite and Improved Flame Retardancy and Mechanical Properties of Flame-Retardant Acrylonitrile-Butadiene-Styrene Composites

Ningjing Wu*, Zhaoxia Xiu

(Key Laboratory of Rubber-Plastics, Ministry of Education / Shandong Provincial Key Laboratory of Rubber-Plastics, Qingdao University of Science & Technology, Qingdao City 266042, People's Republic of China)



Abstract: Surface microencapsulated aluminum hypophosphite (SiAHP) was successfully prepared via the condensation polymerization of *N*-(β -aminoethyl)- γ -aminopropylmethyldimethoxysilane. The notched impact strength of the ABS/SiAHP composites was significantly enhanced compared to the corresponding ABS/AHP composites because the microencapsulated SiAHP improved the compatibility of SiAHP and the ABS matrix, and the vertical burning rate of the ABS composite with only 22.0 wt% SiAHP achieved V-0. The cone

calorimeter tests demonstrated that the peak heat release rate (PHRR) and peak smoke production rate (PSPR) values of the ABS/22wt%SiAHP composite were decreased by 81.1% and 49.5%, respectively, compared to those of the ABS/22wt%AHP composite. Moreover, the total heat release (THR) and the total smoke production (TSR) values of the ABS/SiAHP composites were all lower than those of the ABS/AHP composites. These results clearly indicated that the silicone microencapsulation modification of SiAHP not only enhanced the flame retardancy efficiency of the FR ABS/SiAHP composite but also effectively restrained the smoke production rate of the ABS. A comparison of digital photographs and SEM images of the residues of the ABS/AHP and ABS/SiAHP composites after the cone calorimeter tests revealed that the residue of the ABS/SiAHP composites exhibited a denser and more compact surface char layer structure than that of the ABS/AHP composite. Energy-dispersive X-ray spectroscopy (EDS) measurement indicated that SiAHP more effectively promoted the carbon formation in the FR ABS composite at the surface compared to AHP. The three-dimensional compact char layer network containing C and Si effectively improved the flame retardancy of the ABS/SiAHP composite. Therefore, the flame retardancy of the ABS/SiAHP composite was attributed more to condensed-phase mechanisms than was the flame retardancy of the ABS/AHP composite.

Keywords: aluminum hypophosphite, flame retardancy, surface microencapsulation, Acrylonitrile-Butadiene-Styrene, mechanical property

1. Introduction

ABS (acrylonitrile-butadiene-styrene copolymer) resin is one of the most important thermoplastic materials because of its good mechanical properties, high-impact strength, easy processing and good chemical resistance; it is widely used in the electronics and electricity industries as well as in automobile, building and household fields. However, its inherent flammability restricts its widespread application of this material. Thus the addition of flame retardants is an effective method to improve the flame retardancy of ABS materials¹⁻². In recent years, halogen-free flame retardants based on phosphorus, silicon, nitrogen, and other elements have attracted considerable attention as a result of health and environmental concerns³⁻⁷. Therefore, developing various halogen-free flame retardants with multiple adaptabilities and high flame retardant efficiency is an important topic in the field of flame retarded materials.

Hypophosphite salts and salts of alkylphosphinic acid have been used as new effective flame retardants because they exhibit good flame retardant properties, thermal stability and water resistance⁸⁻²². The salts of alkylphosphinate and hypophosphite are promising flame retardants for applications in engineered plastics and other heterochain polymers, such as poly(1,4-butylene terephthalate (PBT)⁸⁻¹⁰, polyamide-6 (PA6)¹¹⁻¹², polyamide 66 (PA66)¹³, polylactic acid (PLA)¹⁴⁻¹⁶, polyvinyl alcohol (PVA)¹⁷, polyurethane (PU)¹⁸. The combination of different flame retardant systems, including aluminum hypophosphinic acid and the alkyl phosphinic acid salt¹⁹, aluminum phenyl hypophosphinic acid and melamine polyphosphate²⁰⁻²¹, melamine phosphate and ammonium phosphate and zinc borate composite¹³,

effectively improved the flame retardancy of glass-fiber reinforced polyamide 6 (GFPA6) and polyamide 66 (GPPA66). The flame retarded poly(butylene succinate) (PBS) in combination with silica as a synergistic agent exhibited good flame retardancy and antidripping properties²². The combinations of aluminum hypophosphate (AHP) and melamine cyanurate²³, aluminum hypophosphate and metal oxide²⁴, aluminum hypophosphate and POSS²⁵ have also enhanced the flame retardant efficiency of FR PBT or FR PET composites.

Because of the low flame retardancy efficiency of the polyolefin, there are few literatures about salts of alkylphosphinic acid and hypophosphite salts employed as flame retardants on polyolefin. Aluminum hypophosphate (AHP) was ever used in the flame retardant polystyrene (PS)²⁶ and ethylene-propylene-diene monomer rubber (EPDM)²⁷. When the content of AHP reached 25 wt%, the LOI of PS/AHP composite was 25.6% and it passed UL-94 V-0 rating. The incorporation of nanosilica improved the flame-retardancy and the mechanical properties of the EPDM/AHP composite. Three metal hypophosphites, including aluminum hypophosphite (AP), magnesium hypophosphite (MP), and calcium hypophosphite (CP) were applied to flame retarded ABS. The results indicated that AHP could endow the best flame retardancy for ABS with a UL-94 V-0 rating and LOI value of 25.1%. The flame-retardant mechanism was attributed to the formation of a two-layer protective barrier consisting of an organic P-O-C char layer and inorganic layer to insulate material from fire and oxygen in the condensed phase, and the generation of PO \cdot and P \cdot to capture the reactive radicals in the vapor phase²⁸. In our previous paper, ABS composites with

aluminum hypophosphite (AHP) and different synergistic agents presented good flame retardancy and different synergistic flame retardancy mechanisms²⁹. Because AHP is one kind of inorganic phosphorous-containing flame retardant, its surface property is different from ABS matrix, thus the incompatibility of ABS matrix and AHP and uneven dispersion of AHP particles in ABS matrix leads to the great decrease of toughening property of FR ABS/AHP composites. In addition, toxic gases, such as PH₃, are released during the decomposition of AHP. These issues have thus hindered the development of hypophosphite salts in flame retardant polyolefins. Therefore, modifying the surface of aluminum hypophosphinate and improving the compatibility between the flame retardant and the polymer are important for the large-scale application and development of the hypophosphinate salt in the high-performance flame retardant polyolefins.

The surface microencapsulated modification of flame retardants has been demonstrated to be an effective method for improving the interfacial adhesion between the polymer matrix and the flame retardant³⁰⁻³². Microencapsulated red phosphorus using melamine cyanurate not only exhibited high flame retardant efficiency but also improved the compatibility between the PA66 or GFPA66 matrix and the flame retardant³³. Moreover, the microencapsulation of red phosphorus using melamine-formaldehyde also reduced the solubility of the phosphorus in water and reduced the emission of phosphine (PH₃) during the burning process³⁴. Microencapsulated magnesium hydroxide modified with urea formaldehyde and melamine formaldehyde resins greatly improved the flame retardancy of EVA³⁵.

Microencapsulated ammonium polyphosphate modified with melamine formaldehyde resin altered the flame retardancy mechanisms and improved the mechanical properties of PP³⁶.

The study of microencapsulated salts of alkylphosphinic acid and hypophosphite has rarely been reported. In this study, aluminum hypophosphite (AHP) was microencapsulated by *N*-(β -aminoethyl)- γ -aminopropylmethyl siloxane with the aim of enhancing both the flame retardancy efficiency of AHP and the compatibility between the ABS matrix and AHP. The structure of silicone microencapsulated-aluminum hypophosphite (SiAHP) was characterized by Fourier transform infrared spectroscopy (FTIR), thermogravimetric analysis (TGA) and Transmission electron microscopy (TEM) measurements. The mechanical properties and morphologies of the FR ABS/AHP composites and FR ABS/SiAHP composites were compared. The flame retardancy of the FR ABS composites was systematically investigated using a limiting oxygen index (LOI) test, a UL-94 test and a cone calorimeter test. Scanning electron microscopy (SEM) and energy-dispersive X-ray spectroscopy (EDS) measurements were further used to investigate the flame retardancy mechanisms of ABS/SiAHP composites.

2. Experimental

2.1 Materials. ABS resin (GP22, A:B:S=20:30:50, BASF China Co., Ltd.) in granular form was purchased from Qingdao Laiken Corp. Co. in China. AHP (purity \geq 99.0%, average size \leq 5 μ m) was purchased from Qingdao Fusilin Chemical and Technology

Corp. in China. *N*-(β -Aminoethyl)- γ -aminopropylmethyldimethoxysilane (Si-602) was purchased from Qufu Chenguang Chemical Co., Ltd. in China.

2.2 Microencapsulated modification of AHP

N-(β -Aminoethyl)- γ -aminopropylmethyldimethoxysilane (Si-602), ethanol and deionized water were mixed in a constant pressure funnel. The silane mixture solution was gradually dripped into the AHP and reacted in a three-neck flask for 3 h at 60 °C. The procedures were described in our previous paper³⁷. The resulting product was washed with deionized water and dried under vacuum pressure at 80 °C. The obtained product was white powder. The reaction schematic of surface microencapsulated aluminum hypophosphite (SiAHP) is shown in Figure 1. The SiAHP particles were characterized by TEM, as shown in Figure 2. The average size of the SiAHP particles was approximately 1.0 μ m, and the thickness of microencapsulation was not uniform, with a maximum thickness of approximately 300 nm.

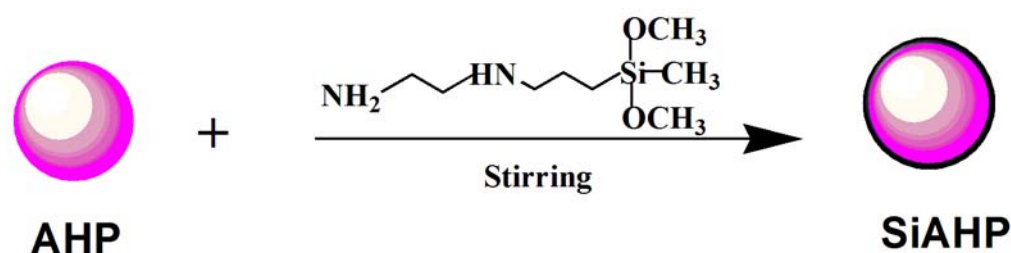


Figure 1. Reaction schematic of surface microencapsulated aluminum hypophosphite (SiAHP).

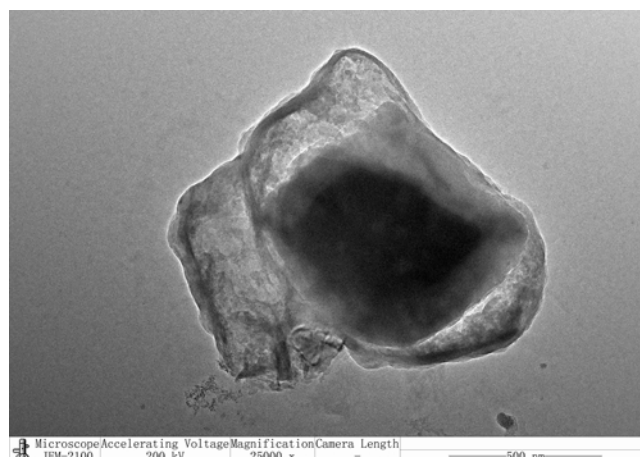


Figure 2. TEM image of SiAHP particles.

2.3 Preparation of flame-retardant ABS composites

ABS, AHP and SiAHP were dried in an oven at 80 °C for 4 h before use. The flame retardants and the ABS resin were blended in a high speed mixer, and then the ABS and flame retardants were subsequently melt-extruded in a CTE-20 type twin-extruder (Nanjing Kebeilong Machinery Co., Ltd, China) in the temperature range from 180 °C to 210 °C and at a twin-screw rotation speed of 50 rpm. The extrudates were cooled and cut into pellets. The pellets were dried at 80 °C in an oven for 4 h, and injected and molded into standard samples for mechanical property measurements in the molding machine at an injection temperature range of 185 °C to 230 °C. Some pellets were hot-pressed under 10 MPa for 10 min at 200 °C to obtain 3.2 mm thick plaques and were subsequently cut into standard samples for flame retardancy measurements of the ABS composites.

2.4 Measurements.

FT-IR spectra of AHP and SiAHP were recorded on a Vector 33 FTIR

spectrophotometer (Bruker Co., Germany) using KBr disks in the wavenumber range of 400-4000 cm^{-1} .

Thermogravimetric Fourier-transform infrared spectroscopy (TG-FTIR) measurements of the samples were performed using a TGA-7 type thermo-analysis instrument (Perkin-Elmer Co., USA) linked to the Vector 33 FTIR spectrophotometer (Bruker Company, Germany). The samples were measured in an alumina crucible with a mass of approximately 5.5 ± 0.3 mg; the measurements were performed from room temperature to 800 $^{\circ}\text{C}$ at a heating rate of 10 $^{\circ}\text{C}/\text{min}$ under a nitrogen atmosphere.

Flexural tests were conducted according to GB/T 9341-2000. Tensile tests were conducted at a crosshead speed of 20 mm/min according to GB/T 1040.1-2006. The Izod impact properties were tested according to GB/T 1843-2008 and the depth of the nick was 2 mm.

The limited oxygen index (LOI) was measured using a HC-2 oxygen index meter (Jiangning Analysis Instrument Co., China) according to the standard oxygen index test ASTM D2863. The specimen dimensions were $130 \times 6.5 \times 3.2$ mm^3 .

UL94 vertical burning tests were performed using a vertical burning instrument (CFZ-1 type, Jiangning Analysis Instrument Co., China) according to UL94 test ASTM D3801-2010. The dimensions of the samples were $130 \times 13 \times 3.2$ mm^3 .

The cone-calorimeter tests were performed on a cone calorimeter (Fire Testing Technology, U.K.) according to ASTM E1354/ISO 5660. The dimensions of the

samples were $100 \times 100 \times 3.2 \text{ mm}^3$. Each specimen was wrapped in aluminum foil and exposed horizontally to a 50 kW/m^2 external heat flux.

Scanning electron microscopy (SEM) was used to observe the surface and inner morphologies of the residue samples obtained from the cone-calorimeter tests. The observations were performed on a JSM-6700F (Japan Electronics Corp.) scanning electron microscope. The specimens were coated with a conductive layer of gold prior to imaging.

Energy-dispersive X-ray spectroscopy (EDS) was performed to obtain the relative elemental compositions of the residue samples at the surface and inner obtained from the cone-calorimeter test using an EDS apparatus (INCA type, British Oxford Instrument Co.).

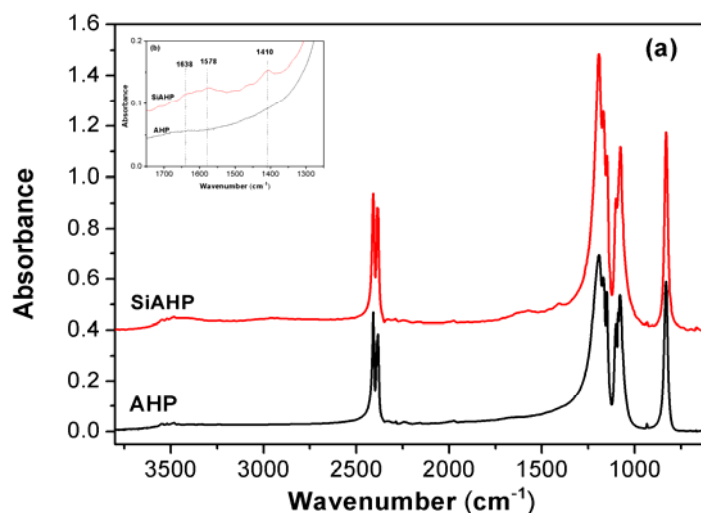
Transmission electron microscopy (TEM) was conducted to investigate the microstructures of the microencapsulated SiAHP using a JEM-2100 (Japan Electronics Corp.) transmission electron microscope. The specimens were prepared in 0.1% (w/w) water dispersion and dropped onto copper grids.

3. Results and discussion

3.1 Characterization of Surface Microencapsulated AHP

The surface of AHP was microencapsulated by the condensation polymerization of *N*- β -aminoethyl- γ -aminopropylmethyldimethoxysilane. The FT-IR spectra of AHP and modified AHP (SiAHP) are shown in Figure 3. The typical absorption peak of AHP at 2400 cm^{-1} corresponds to the stretching vibration of P-H. The characteristic

peak at 1256 cm^{-1} is ascribed to the stretching vibration of $\text{P}=\text{O}$. Compared to the FT-IR spectrum of AHP, the FT-IR spectrum of SiAHP exhibits the characteristic absorption bands at 3480 cm^{-1} for N-H stretching vibration in Figure 3(a). The absorption signals of $-\text{NH}_2$, $-\text{NH}$ and $-\text{CH}_2$ for SiAHP are very weak, the enlarged FT-IR spectra are shown in Figure 3(b). The characteristic peaks at 1638 cm^{-1} and 1578 cm^{-1} are ascribed to the N-H stretching vibrations and 1410 cm^{-1} is ascribed to the CH_2 stretching vibration of silicone. In Figure 3 (c), the enlarged FT-IR spectra of AHP and SiAHP in the range of $1200\text{--}1000\text{ cm}^{-1}$ exhibit the different characteristic absorption bands. The characteristic absorption band at 1076 cm^{-1} is ascribed to the Si-O stretching vibrations of silicone, and the characteristic absorption bands at 1101 cm^{-1} and 1079 cm^{-1} are assigned to the overlap bands of P-O stretching vibrations and Si-O stretching vibrations of SiAHP. The FT-IR and TEM results indicated that *N*-(β -aminoethyl)- γ -aminopropylmethyl silicone was grafted at the surface of AHP to form the silicone microencapsulation.



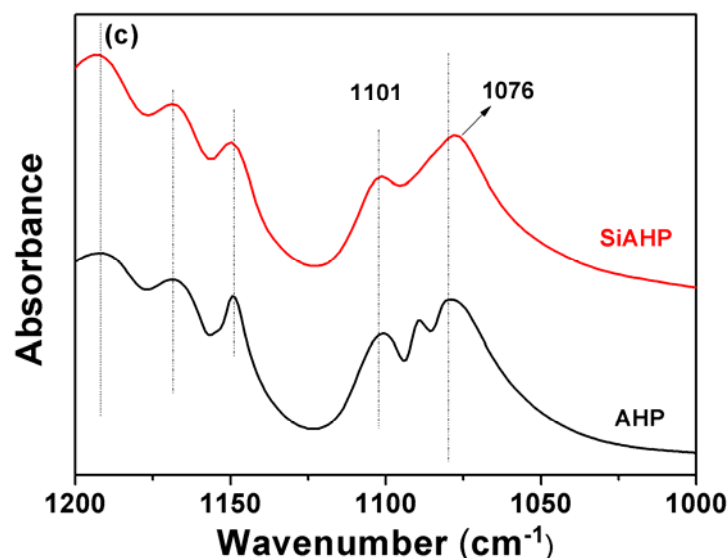


Figure 3. (a) FT-IR spectra of AHP and SiAHP particles. (b) Enlarged FT-IR spectra in the range of 1750-1250 cm^{-1} , (c) 1200-1000 cm^{-1} .

Thermal degradation analysis curves of AHP and SiAHP under a nitrogen atmosphere are shown in Figure 4 and the related data are listed in Table 1. The onset decomposition temperatures ($T_{5\%}$) of AHP and SiAHP were 327.2 °C, and 319.0 °C, respectively. AHP exhibited three temperatures of the maximum weight-loss rate (T_{max}): 339.9, 422.3 and 454.9 °C, whereas SiAHP exhibited two T_{max} at approximately 333.9 and 427.1 °C in Figure 4 (b). The residue of SiAHP at 700 °C was 76.4%, which was higher than that of AHP. These results indicated that the incorporation of the silicone microencapsulation minimally influenced on the thermal stability of SiAHP.

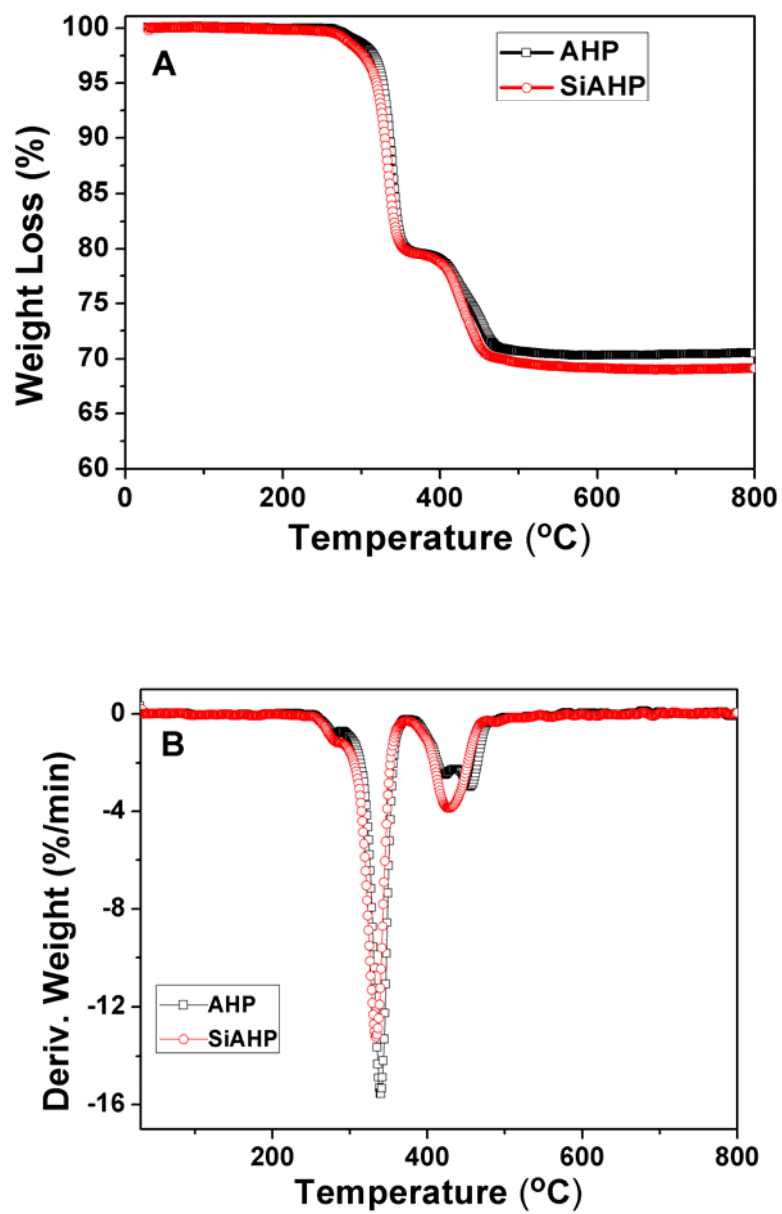


Figure 4. TGA (A) and DTG (B) curves of AHP and SiAHP in a nitrogen atmosphere (heating rate: 10°C/min).

Table 1. TGA Data of Flame retardants and Flame-Retarded ABS Composites.

Samples	T _{5%} (°C)	T _{max1} (°C)	T _{max2} (°C)	T _{max3} (°C)	Total residue yield at 700 °C (wt%)
AHP	327.2	339.9	422.3	454.9	75.2
SiAHP	319.0	333.9	427.1	-	76.4
ABS/25wt%AHP	360.3	355.2	443.3	-	19.9
ABS/25wt%SiAHP	344.4	338.3	440.3	-	20.3

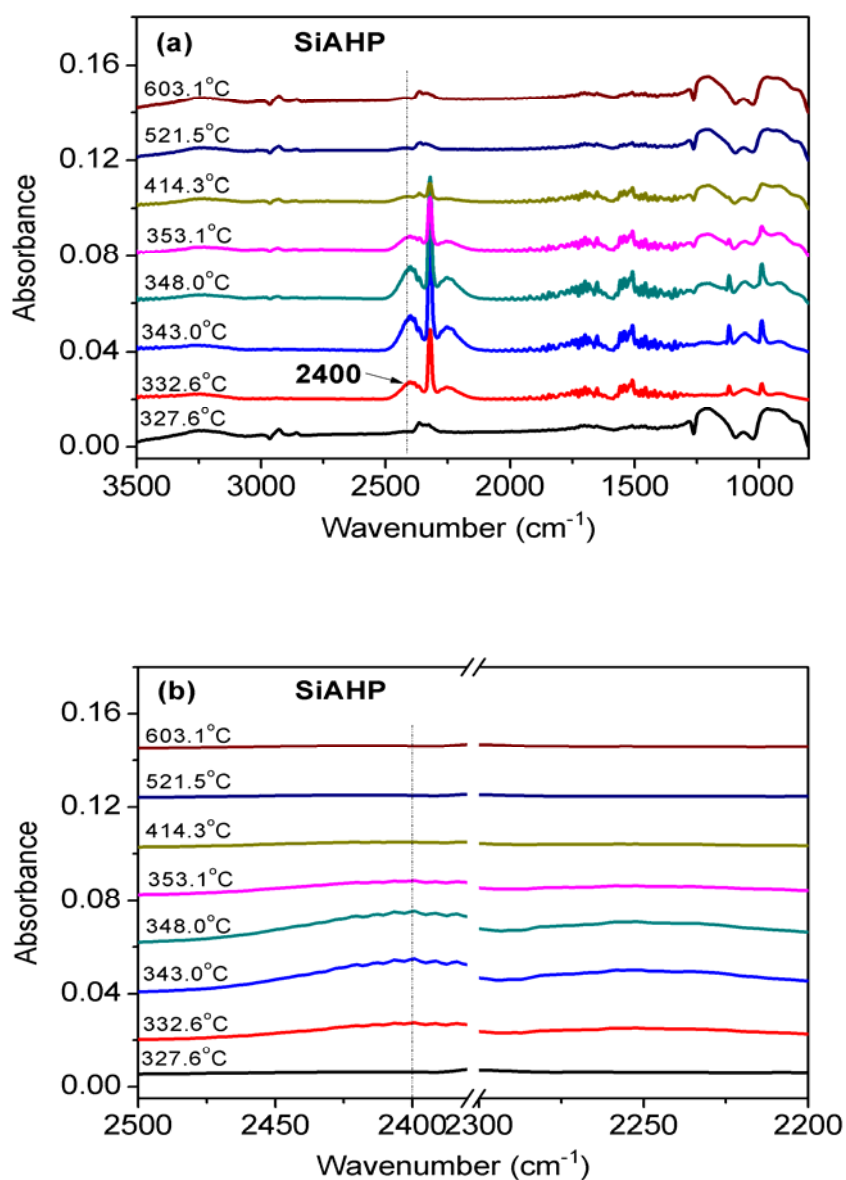


Figure 5. TG-FTIR spectra of gaseous product of SiAHP in the thermal degradation

process (a) 3500-800 cm⁻¹, (b) 2500-2200 cm⁻¹.

TG-FTIR measurements that provide direct identification of the evolved gaseous products contribute to the understanding of the influence of the silicone microencapsulation modification on the thermal degradation process of AHP. The FT-IR spectra of the thermal decomposition gaseous products for SiAHP are shown in Figure 5 (A). The characteristic peak of P-H at 2400 cm^{-1} appeared at $332.6\text{ }^{\circ}\text{C}$, and the peak intensity increased with increasing temperature. To clearly observe the thermal decomposition process of SiAHP, the spectra of SiAHP were enlarged in Figure 5(B) in the range of $2600\text{-}2200\text{ cm}^{-1}$ and eliminated the influence of CO and CO₂ during the TGA measurements. When the temperature was increased to $348.0\text{ }^{\circ}\text{C}$, the characteristic peak intensity at 2400 cm^{-1} reached approximately maximum, which was attributed to the further release of PH₃ at the thermal decomposition stage of AHP. When the temperature was increased to $414.3\text{ }^{\circ}\text{C}$, the characteristic peak intensity decreased because of the decrease in the released amount of PH₃. Compared to the reported literatures^[28-29], the silicone microencapsulation modification of SiAHP has little influence on the thermal degradation process of AHP.

3.2 Thermogravimetric Analysis and Mechanical Properties of Flame-Retardant ABS Composites.

The thermal degradation behavior of ABS/25wt%AHP and ABS/25wt%SiAHP composites under nitrogen conditions are compared in Figure 6(a). The T_{5%} of ABS/25wt%SiAHP composite was $344.4\text{ }^{\circ}\text{C}$ and its two T_{max} values were $338.3\text{ }^{\circ}\text{C}$ and $440.3\text{ }^{\circ}\text{C}$, which were slightly lower than the corresponding T_{5%} ($360.3\text{ }^{\circ}\text{C}$) and the two T_{max} values of AHP (T_{max1}: $355.2\text{ }^{\circ}\text{C}$, T_{max2}: $444.3\text{ }^{\circ}\text{C}$) in Figure 6(b). And, the

residue of ABS/25wt%SiAHP composite at 700 °C was 20.3%, which was slightly greater than that of the ABS/25wt%AHP composite. These results indicated that the microencapsulated modification of SiAHP minimally influenced on the thermal stability of the FR ABS composite, and SiAHP effectively promoted the char formation of ABS during the thermal decomposition, which was beneficial for improving the flame retardancy of the FR ABS composite.

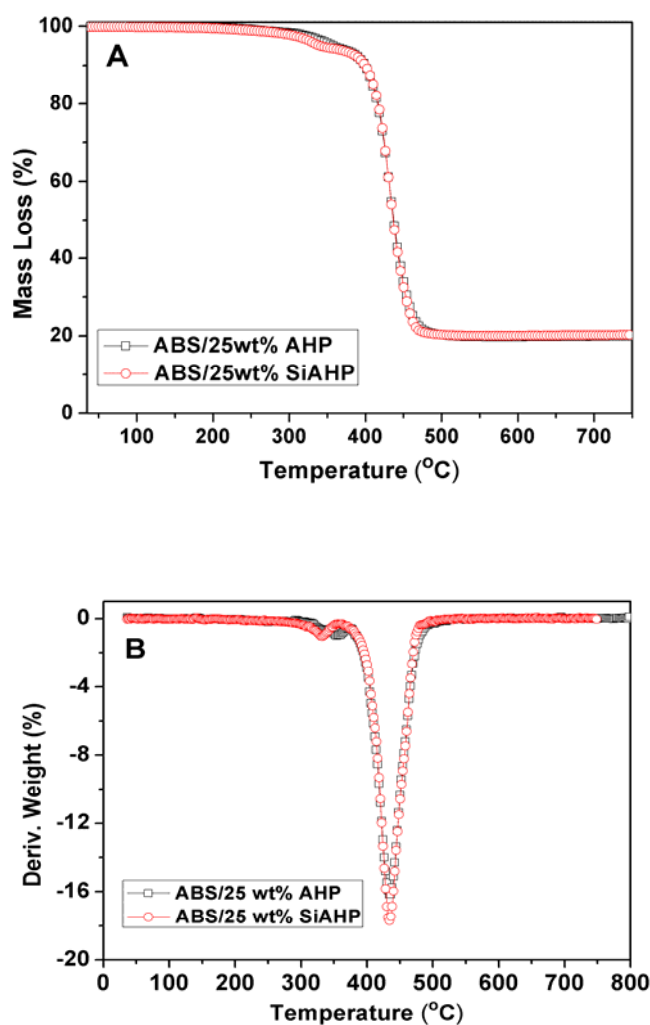


Figure 6. TGA (A) and DTG (B) curves of ABS/ AHP and ABS/SiAHP composites in a nitrogen atmosphere (heating rate: 10°C/min).

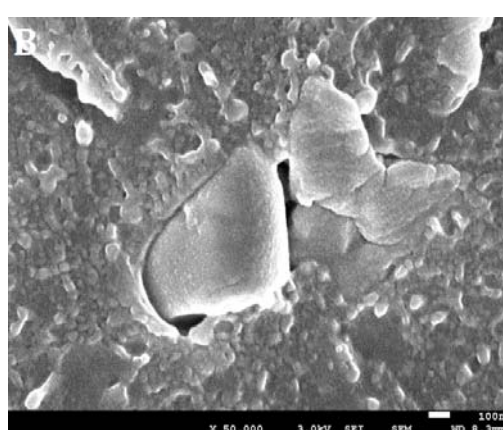
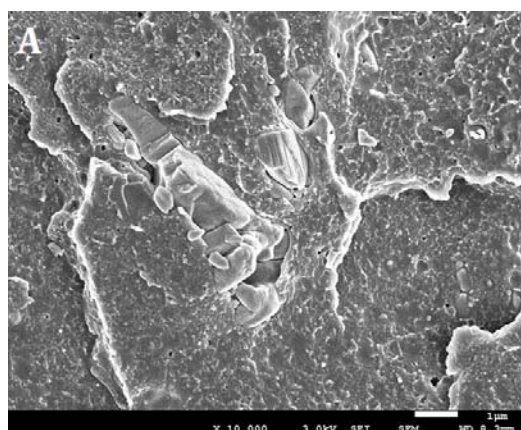
The mechanical properties of the ABS and FR ABS composites are listed in Table 2. Compared to the tensile strength and flexural strength of neat ABS, those of the FR ABS composites with 22 wt% and 25 wt% AHP exhibited no obvious changes, whereas the tensile strength and flexural strength of the FR ABS composites with 22.0 wt% and 25.0 wt% SiAHP exhibited a slight increase. However, the notched impact strength and the elongation yield at break of ABS/AHP composite dramatically decreased. In addition, the notched impact strength of the ABS/22wt%SiAHP composite dramatically increased from 3.3kJ/m² of ABS/22wt%AHP composite to 7.5 kJ/m². Similarly, the notched strength for the FR ABS composite with 25.0 wt% SiAHP improved by approximately twofold compared to that of the ABS/25.0wt% AHP composites. These results indicated that the silicone microencapsulation of SiAHP promoted the enhancement of the notched impact strength of the ABS/SiAHP composites.

To investigate the effect of microencapsulated SiAHP on the mechanical properties of the FR ABS composites, we observed the surface morphologies of the ABS/25wt%AHP and ABS/25wt%SiAHP composites at the fracture using SEM analysis. As shown in Figure 7, the bright and irregular AHP particles were dispersed in the ABS/AHP composites and most of AHP particles were aggregated in the FR ABS composites in Figure 7(A). The dimensions of the AHP white particles were determined to be from 500 nm to 1µm and the interface between AHP particles and ABS matrix was clear, as shown in Figure 7(B). In the case of the ABS/25wt%SiAHP composites, most of SiAHP particles were relatively uniformly dispersed in the ABS

matrix in Figure 7(C). The dimensions of the white AHP particles were about 500 nm and the interface between SiAHP particles and ABS matrix was vague, as shown in Figure 7(D). These results indicated that the silicone microencapsulation modification of SiAHP improved the dispersion in ABS matrix and enhanced the interfacial adhesion between the flame retardant and the ABS matrix. It is considered that the amino group of silicone and the cyano group of the ABS matrix have similar polarities, which promoted the improvement of the compatibility between the ABS matrix and the SiAHP particles.

Table 2. Mechanical properties of ABS and FR ABS composites.

Sample	Flexural strength (MPa)	Tensile strength (MPa)	Elongation yield at break (%)	Notched impact strength (kJ/m ²)
ABS	62.6±0.5	38.0±0.6	10.0±1.5	17.0±0.3
ABS/22wt%AHP	63.1±0.4	37.6±0.4	2.0±0.2	3.3±0.2
ABS/25wt%AHP	61.1±0.5	36.1±0.3	1.4±0.1	2.1±0.3
ABS/22wt%SiAHP	64.5±0.3	39.5±0.5	2.1±0.1	7.5±0.3
ABS/25wt%SiAHP	64.7±0.4	38.2±0.4	2.0±0.2	6.9±0.2



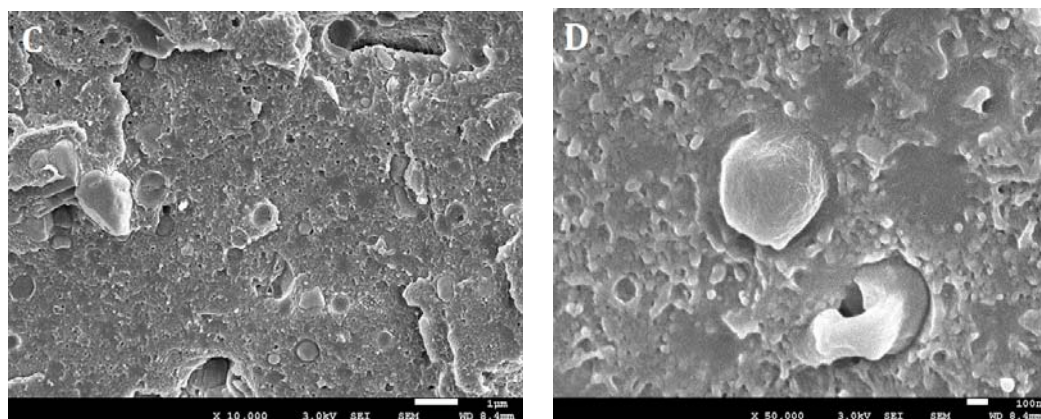


Figure 7. SEM images of FR ABS composites at the fracture (A) ABS/25wt%AHP composite, magnification: 1×10^4 , (B) ABS/25wt%AHP composite, magnification: 5×10^4 , (C) ABS/25wt%SiAHP composite, magnification: 1×10^4 , ABS/25wt%SiAHP composite, magnification: 5×10^4 .

3.3 Flame Retardancy of FR ABS/AHP Composites

LOI, UL-94 and cone calorimeter tests are widely used to determine the flammability of flame retardant materials. The LOI values and UL-94 test results of the flame-retarded ABS composites are presented in Table 3. With the addition of 22 wt% AHP, the results showed that the ABS composite achieved a V-1 rating and its LOI value was 24.5%. For the ABS/22.0wt%SiAHP composite, the vertical burning rate achieved V-0 and the LOI value was improved to 25.0%. Moreover, the smoke density was also lower than that of the ABS/22wt%AHP composite. When the SiAHP content was increased to 25wt%, the vertical burning rate of the FR ABS composite achieved V-0 and the LOI value was increased to 25.5%. The flame retardancy of the ABS/SiAHP composite was clearly greater than that of the ABS composite with the same amount of AHP, indicating that the flame retardancy of the ABS/SiAHP composite was enhanced by the surface silicone

microencapsulation modification of SiAHP.

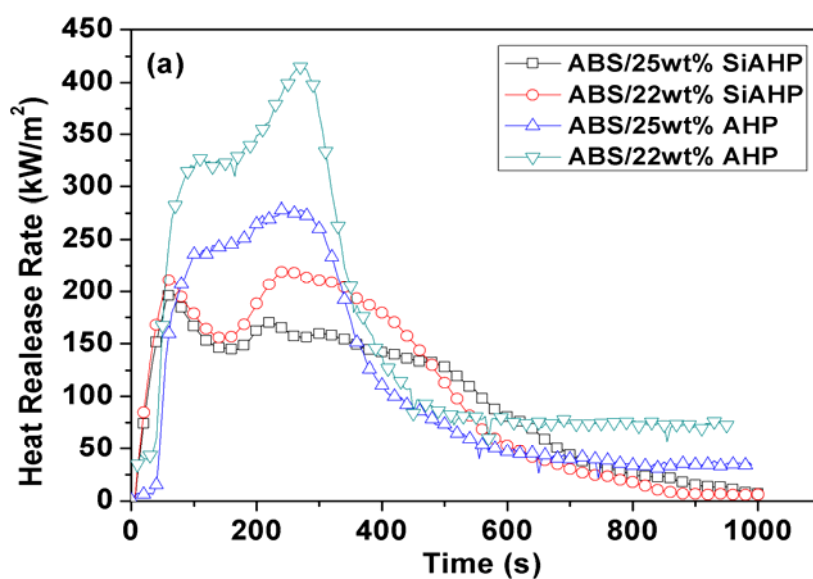
Table 3. LOI values and UL-94 results of ABS/AHP and ABS/SiAHP composites.

Samples	ABS (wt%)	AHP (wt%)	SiAHP (wt%)	LOI (%)	UL-94 classes	Smoke
ABS/22wt%AHP	78	22		24.5	V-1	light
ABS/25wt%AHP	75	25		25.0	V-0	light
ABS/22wt%SiAHP	78		22	25.0	V-0	lighter
ABS/25wt%SiAHP	75		25	25.5	V-0	lighter

The cone-calorimeter test data for the flame retardant ABS composites are listed in Table 4. The peak heat release rate (PHRR) value of the ABS/22wt%SiAHP composite was 213.7 kW/m². With the increasing of SiAHP content, the PHRR value of the ABS/25wt%SiAHP composite was decreased to 195.0 kW/m², which was reduced by 68.6% compared to that of the ABS/25wt%AHP composite. The heat release rate (HRR) and total heat release (THR) curves of the flame retardant ABS are shown in Figure 8. It clearly indicated that the HRR and THR values of the ABS/SiAHP composites were decreased with the increasing of SiAHP content in Figure 8(A) and Figure 8(B). Moreover, with the incorporation of SiAHP, the T_{PHRR} values of the ABS/22wt%SiAHP and ABS/25wt%SiAHP composites were delayed to 265.0 s and 307.5 s, respectively. These cone-calorimeter test data indicated that surface microencapsulated SiAHP could effectively enhance the flame retardancy of ABS composites.

Table 4. Cone Calorimeter Test Data for ABS/AHP and ABS/SiAHP composites.

Sample	ABS/22wt%	AHP/25wt%	ABS/22wt%	ABS/25wt%
	AHP	AHP	SiAHP	SiAHP
TTI (s)	12.5±0.5	12.0±1.0	11.5±0.5	13.0±1.0
PHRR (kW/m ²)	387.0±27.7	279.5±1.0	213.7±7.8	195.0±2.5
T _{PHRR} (s)	245±15.0	257.5±12.5	265.0±5.0	307.5±7.5
THR (MJ/m ²)	125.8±14.2	99.0±9.5	101.6±5.6	96.5±5.2
PMLR (g/s)	0.172±0.005	0.171±0.005	0.129±0.002	0.139±0.001
CR (%)	12.3±1.6	13.0±0.3	20.8±0.1	23.0±0.1
PSPR (m ² /s)	0.139±0.002	0.130±0.005	0.093±0.002	0.086±0.002
FGR (kW/(m ² /s))	1.58	1.09	0.80	0.54



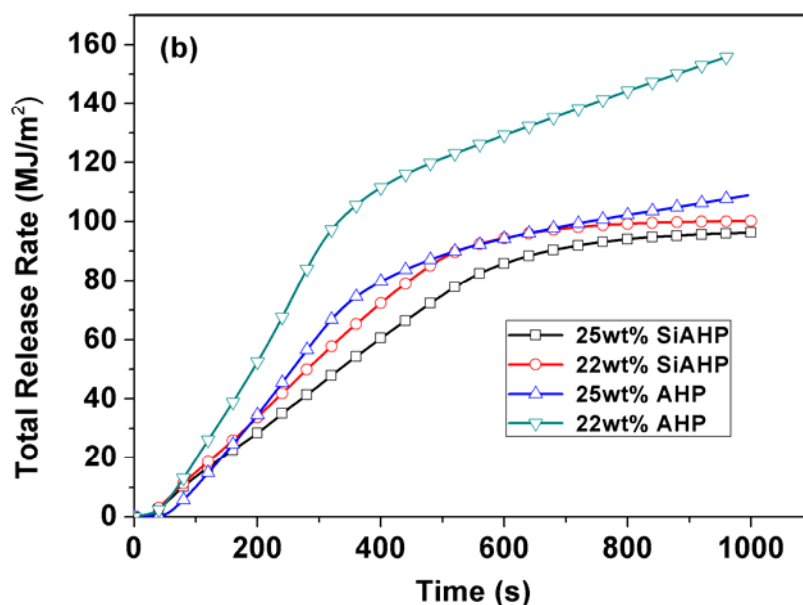


Figure 8. HRR (a) and THR (b) curves of ABS/AHP and ABS/SiAHP composites during the cone calorimeter test.

The peak mass loss rate (PMLR) value of ABS composite with 22wt% SiAHP was 0.129 g/s, as shown in Table 4, which was approximately reduced by 25% compared to that of ABS/22wt%AHP composite. The char residue yield (CR) curves of the FR ABS composites are shown in Figure 9. The CR values of the ABS/22wt%SiAHP composite after the cone calorimeter test was 20.8%. With the increasing of SiAHP content, the CR value of the ABS/SiAHP composites was increased to 23.0%, which was increased by 43.5% compared to that of ABS/25wt%AHP composites. These results indicated that the silicone microencapsulated SiAHP effectively promoted the formation of the residues of the FR ABS composites.

The smoke production rate (SPR) and total smoke production (TSP) curves of flame

retardant ABS are shown in Figure 10. For FR ABS/SiAHP composites, the TSR values of the FR ABS composites were decreased with the increasing of SiAHP content, and the TSR values of ABS/22wt%SiAHP and ABS/25wt%SiAHP composites were lower than those of the ABS/AHP composites with the same flame retardant content. As shown in Table 4, the peak smoke production rate (PSPR) values of the ABS/22wt%SiAHP and ABS/25wt%SiAHP composites was 0.093 m²/s and 0.086 m²/s, which represented reductions of approximately 49.5% and 51.2% compared to those of ABS/22wt%AHP and ABS/25wt%AHP composites, respectively. These results demonstrated microencapsulated SiAHP more efficiently suppressed the smoke production of ABS composites compared to AHP in the FR ABS composites.

Generally, a lower fire growth rate (FGR) value indicates that the time to flashover is delayed. For the ABS/22wt%SiAHP composite, the FGR value was 0.80 kW/(m²·s). With the increasing of AHP content, the FGR value of ABS/25wt%SiAHP composites was decreased to 0.54 kW/(m²·s), which was reduced by 101.9% compared to that of the FR ABS composites with the same amount of AHP, respectively. Therefore, the microencapsulation modification of SiAHP greatly reduced the FGR of the ABS/SiAHP composite. These results demonstrate that SiAHP effectively improved the fire safety of FR ABS composite.

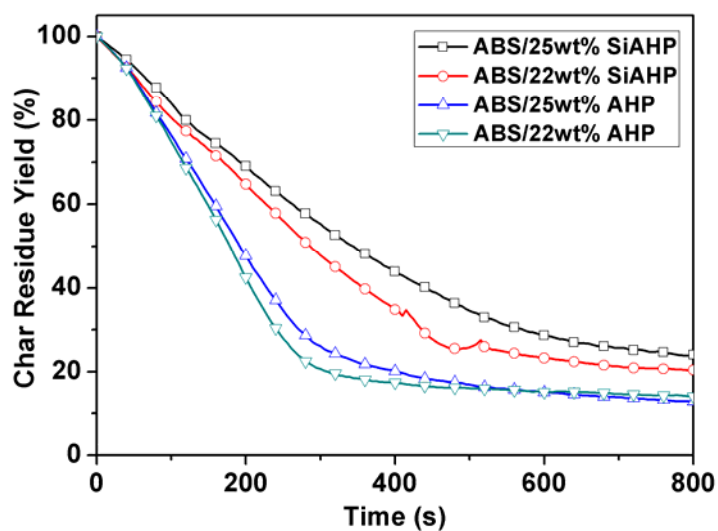


Figure 9. Char residue yield curves of ABS/AHP and ABS/SiAHP composites during the cone calorimeter test.

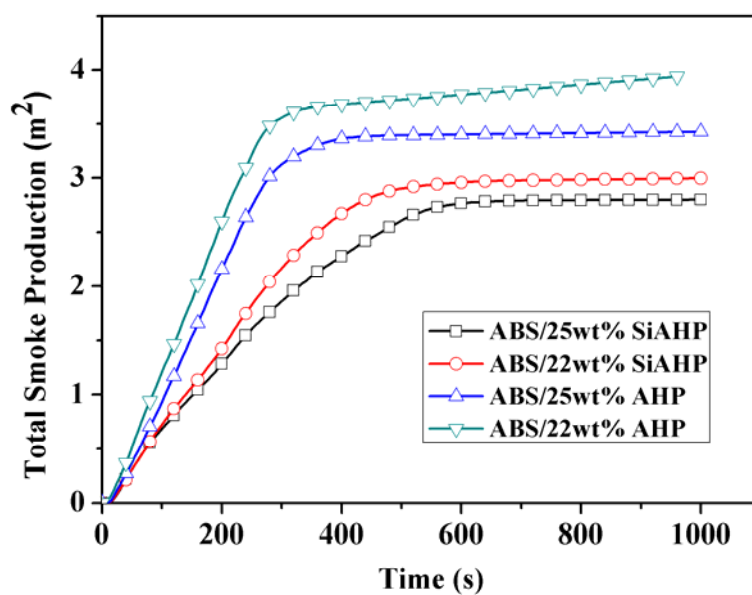


Figure 10. TSR curves of ABS/AHP and ABS/SiAHP composites during the cone calorimeter test.

3.4 Morphologies of Residues and Flame Retardancy Mechanism

To further investigate the influence of SiAHP on the flame retardancy mechanism, the morphologies of the residues of the ABS/AHP and ABS/SiAHP composites were observed. Digital photos of the residues for the ABS/AHP and ABS/SiAHP composites after the cone calorimeter test are shown in Figure 11. In the case of the ABS/22wt%AHP composites, the residue exhibited an obvious char layer structure; in addition, numerous intervals were observed between the residue layers in Figure 11(A). When the content of AHP was increased to 25 wt%, the char residue appeared thicker and the intervals between residue layers became narrower than those of ABS/22wt%AHP in Figure 11(B). In the case of the ABS/SiAHP composites, we observed that the morphologies of the residues differed substantially from those of the FR ABS composite with the same amount of AHP, as shown in Figures 11(C) and 11(D). A very compact and uniform surface morphology was observed for the char residue. When the content of SiAHP was increased to 25 wt%, the surface morphology of the char residue appeared more uniform and compact. This result indicated that the silicone microencapsulation modification of SiAHP obviously influenced on the morphology of the formed residues and affected the flame retardancy mechanism of the ABS/SiAHP composites.

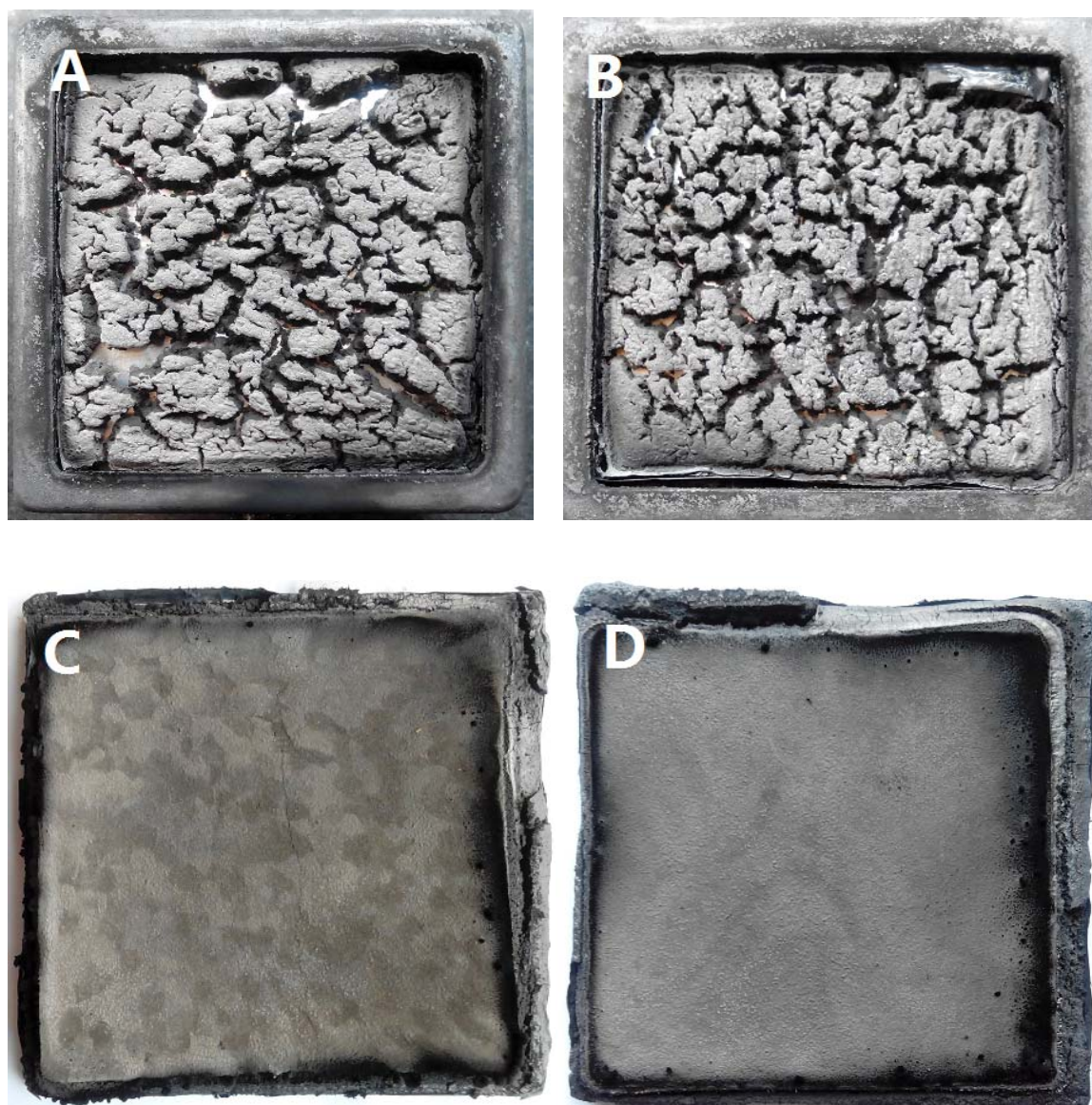


Figure 11. Digital photographs of the residues of FR ABS composites after cone calorimeter test. (A) ABS/22wt%AHP (B) ABS/25wt%AHP (C) ABS/22wt% SiAHP (D) ABS/25wt%SiAHP.

The surface and inner microstructure of the residues of the ABS/25wt%SiAHP composites were further compared by SEM analysis. Figure 12(A) shows the surface morphology of the residue of ABS/25wt%SiAHP composite at 1×10^4 magnification after the cone calorimeter test. Compact and dense char layers with many relatively small cluster-particles were observed. There were some microvoids with the dimension of

approximately 0.5-2 μm . In the 3×10^4 magnification micrograph in Figure 12(A), numerous small particles were closely accumulated and connected into semi-continuous network structure, *and the dimensions of these particles were approximately 200-300 nm* in Figure 12(B). From the literatures³⁸, these small particles were speculated to be generated from the carbonized product of ABS, indicating that the addition of SiAHP promoted the formation of small carbon particles at the surface of the ABS resin. The compact surface microstructure of the residue was more effective in inhibiting the propagation of oxygen and heat into the interior polymer. Figure 12(C) shows the inner morphology of the ABS/SiAHP composite residue at 5×10^3 magnification. Two different types of particles were distributed in the interior of the char layers. The wrinkled particles were relatively irregular with dimensions from 1 to 5 μm . In the 1×10^4 magnification micrograph in Figure 12(D), many smooth, round particles with dimensions ranging from 100 nm to 2 μm were distributed in the inner residue of the ABS/SiAHP composite. These different particles were speculated to be generated from the pyrolysis product of AHP and a small amount of carbonized product of ABS resin. On the basis of the aforementioned analysis, the residue morphologies at the surface and interior for the ABS/25wt%SiAHP composites were differed substantially. The results showed that the incorporation of silicone-microencapsulated SiAHP strongly influenced on the formation of the surface and inner morphologies of the residue.

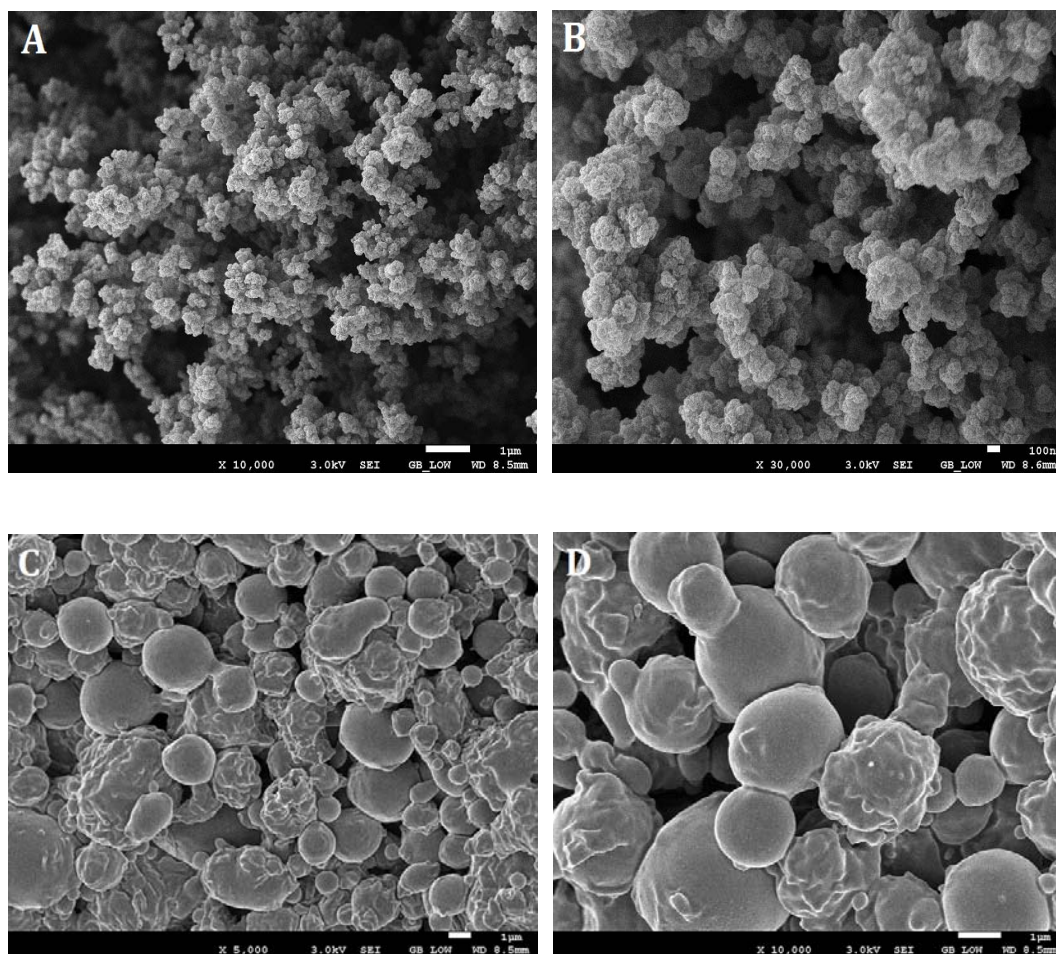


Figure 12. SEM images of the residues of ABS/25wt%SiAHP composites obtained from cone-calorimeter test. (A) surface, magnification: 1×10^4 (B) surface, magnification: 3×10^4 . (C) inner, magnification: 5×10^3 (D) inner, magnification: 1×10^4 .

The chemical components of the surface and inner residual char layers for the ABS/25wt%AHP and ABS/25wt%SiAHP composites after the cone calorimeter test were investigated by EDS analysis, as shown in Table 5. For the ABS/25wt%SiAHP composite, the average relative weight content of C in the residue at the surface was 19.89 wt%, which was higher than that for the ABS/25wt%AHP composite, and the average relative weight percents of O, P and Al in the residue were 39.10 wt%, 32.19

wt% and 7.69 wt%, respectively, which were lower than the corresponding compositions of residue for the ABS/25wt%AHP composite, indicating that the incorporation of the same amount of SiAHP dramatically promoted the carbon element formation of the residue at the surface. At the inner char layer of the residue, the relative composition of C was slightly higher than the corresponding composition of residue for the ABS/25wt%AHP composite. Specifically, the relative weight content of Si of the residue was 1.13 wt%, which was higher than the corresponding composition at the inner layer of the ABS/25wt%SiAHP composite. This result indicated that the silicon-containing component in the residue easily migrated and gathered at the surface during the cone calorimeter test. The three-dimensional compact char residue network containing more C and Si exhibited a more stable structure and effectively improved the flame retardancy of the ABS/SiAHP composite. The flame retardancy mechanism of the ABS/SiAHP composite can therefore be reasonably attributed to the occurrence of more condensed-phase mechanism in the ABS/SiAHP composite than in the ABS/AHP composite.

Table 5. EDS results of residues of ABS/AHP and ABS/SiAHP composites after cone calorimeter test.

Sample		Average Elemental Composition				
		C	O	P	Al	Si
ABS/25wt%AHP (Surface)	wt%	9.31	49.29	31.53	9.83	0
ABS/25wt%AHP (Inner)	wt%	9.11	47.00	32.16	11.73	0
ABS/25wt%SiAHP (Surface)	wt%	19.89	39.10	32.19	7.69	1.13
ABS/25wt%SiAHP (Inner)	wt%	10.09	58.66	21.17	9.62	0.47

4. Conclusions

Microencapsulated aluminum hypophosphite was prepared via the condensation polymerization of *N*-(β -aminoethyl)- γ -aminopropylmethyldimethoxysilane, and its structure was identified by FT-IR and TEM analyses. With the incorporation of SiAHP particles, the mechanical properties of ABS composites showed the notched impact strength of ABS/22wt%SiAHP and ABS/25.0wt%SiAHP improved approximately 1.3 and 2.3-fold, respectively, compared to the corresponding of ABS/AHP composites. SEM analysis results indicated that the microencapsulated SiAHP enhanced the interfacial interaction between the flame retardant and the ABS matrix. The vertical burning test (UL-94) of ABS composite with only 22.0 wt% SiAHP achieved V-0 rating. Cone calorimeter test results showed that the PHRR and PSPR values of ABS/25wt%SiAHP composite were reduced by approximately 68.6% and 51.2%, compared to those of the ABS composite with the same amount of AHP, respectively. These results thus clearly indicated that the surface microencapsulated modification of SiAHP not only enhanced the flame retardancy efficiency of the FR ABS/SiAHP composites, but also effectively restrained the smoke production rate of the FR ABS/SiAHP composites. The digital photographs and SEM images of the residues of FR ABS composite after the cone calorimeter test revealed that the residues of the ABS/SiAHP composites exhibited a denser and more compact surface char layer structure than the ABS/AHP composites. The numerous small carbon-cluster particles were formed at the surface of the residue for ABS/25wt%SiAHP composite after the cone-calorimeter test, and the average relative

weight percents of C and Si of residue at the surface were higher than the corresponding compositions of residue at the inner char layer by the EDS measurement. A higher residue yield and a more compact char layer structure could effectively inhibit the flammable gases from diffusing further into the interior of the polymer. The results indicate that the improvement of the flame retardancy of the ABS/SiAHP composite is attributable to the occurrence of more condensed-phase mechanisms than occurs in the ABS/AHP composite. Therefore, SiAHP is more efficient flame retardant than AHP in improving the flame retardancy of the FR ABS composite.

Address

Key Laboratory of Rubber-Plastics, Ministry of Education Qingdao University of Science & Technology Qingdao City 266042, People's Republic of China

*Corresponding Author: Ningjing Wu

E-mail: ningjing_wu@qust.edu.cn; ningjing_20132013@163.com

Tel. +86-0532-84022420

Acknowledgements

The work was financially supported by the National Natural Science Foundation of China (21104038) and the Scientific Research Foundation of Shandong Province Outstanding Young Scientist Award (2010BSE08010).

Notes and references

1 K. Lee, J. Kim, J. Bae, J. Yang, S. Hong and H. K. Kim, *Polymer* 2002, 43, 2249.

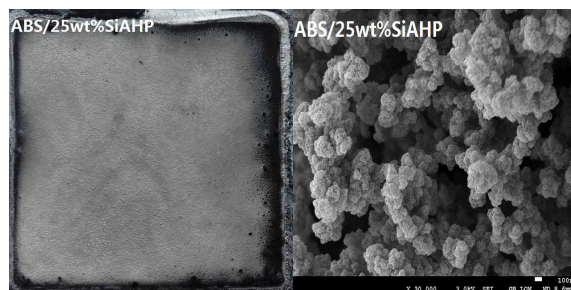
- 2 Y. Y. Ji, J. H. Kim and J. Y. Bae, *J. Appl. Polym. Sci.* 2006, 102, 721.
- 3 Z. B. Shao, C. Deng, Y. Tan, M. J. Chen, L. Chen and Y. Z. Wang, *ACS Appl. Mater. & Interfaces* 2014, 6, 7363.
- 4 B. Li and M. J. Xu, *Polym. Degrad. Stab.* 2006, 91, 1380.
- 5 Z. Z. Xu, J. Q. Huang, M. J. Chen, Y. Tan and Y. Z. Wang, *Polym. Degrad. Stab.* 2013, 98, 2011.
- 6 S. D. Jiang, Z. M. Bai, G. Tang, L. Song, A. A. Stec, T. R. Hull, Y. Hu and W. Z. Hu, *ACS Appl. Mater. & Interfaces* 2014, 6, 14076.
- 7 G. Laufer, C. Kirkland, A. A. Cain and J. C. Crunlan, *ACS Appl. Mater. & Interfaces* 2012, 4, 1643.
- 8 W. Yang, R. K. K. Yuen, Y. Hu, H. Lu and L. Song, *Ind. Eng. Chem. Res.* 2011, 50, 1197.
- 9 W. Yang, Y. Hu, Q. Tai, H. Lu, L. Song and R. K. K. Yuen, *Compos. Part A-Appl. S.* 2011, 12, 794.
- 10 E. Gallo, U. Braun, B. Schartel, P. Russo and D. Acierno, *Polym. Degrad. Stab.* 2009, 94, 1245.
- 11 Q. Li, B. Li, S. Zhang and M. Lin, *J. Appl. Polym. Sci.* 2012, 125, 1782.
- 12 Z. Hu, L. Chen, G. P. Lin, Y. Luo and Y. Z. Wang, *Polym. Degrad. Stab.* 2011, 96, 1538.
- 13 U. Braun, B. Schartel, M. A. Fichera and C. Jäger, *Polym. Degrad. Stab.* 2007, 92, 1528.
- 14 G. Tang, X. Wang, W. Y. Xing, P. Zhang, B. B. Wang, N. N. Hong, W. Yang, Y. Hu and L. Song, *Ind. Eng. Chem. Res.* 2012, 51, 12009.
- 15 G. Tang, X. J. Huang, H. C. Ding, X. Wan, S. D. Jiang, K. Q. Zhou, B. B. Wang, W. Yang and Y. Hu, *RSC Adv.* 2014, 4, 8985.

- 16 G. Tang, R. Zhang, X. Wang, B. Wang, L. Song, Y. Hu and X. L. Gong, *J. Macromol. Sci., Part A: Pure Appl. Chem.* 2013, 50, 255.
- 17 B. H. Yuan, C. L. Bao, Y. Q. Guo, L. Song, K. M. Liew and Y. Hu *Ind. Eng. Chem. Res.* 2012, 51, 14065.
- 18 S. S. Xiao, M. J. Chen, L. P. Dong, C. Deng, L. Chen and Y. Z. Wang *Chinese J. Polym. Sci.* 2014, 32, 98.
- 19 B. Zhao, L. Chen, J. W. Long and Y. Z. Wang, *Ind. Eng. Chem. Res.* 2013, 52, 2875.
- 20 Z. Hu, G. P. Lin, L. Chen and Y. Z. Wang, *Polym. Adv. Technol.* 2011, 22, 1166.
- 21 U. Braun, H. Bahr and B. Schartel, *e-Polym.* 2010, 10, 1.
- 22 Y. J. Chen, J. Zhan, P. Zhang, S. B. Nie, H. D. Lu, L. Song and Y. Hu, *Ind. Eng. Chem. Res.* 2010, 49, 8200.
- 23 U. Braun, H. Bahr, H. Sturm and B. Schartel, *Polym Adv Technol.* 2008, 19, 680.
- 24 E. Gallo, U. Braun, B. Schartel, P. Russo and D. Acierno, *Polym. Degrad. Stab.* 2009, 94, 1245.
- 25 A. Vannier, S. Duquesne, S. Bourbigot, A. Castrovinci, G. Camino and R. Delobel, *Polym. Degrad. Stab.* 2008, 93, 818.
- 26 Y. W. Yan, J. Q. Huang, Y. H. Guan, K. Shang, R. K. Jian and Y. Z. Wang, *Polym. Degrad. Stab.* 2014, 99, 35.
- 27 Z. T. Wang, X. Zhang, C. Bao, Q. Y. Wang, Y. Qin and X. Y. Tian, *J. Appl. Polym. Sci.* 2012, 124, 3487.
- 28 R. K. Jian, L. Chen, B. Zhao, Y. W. Yan, X. F. Li, Y. Z. Wang. *Ind. Eng. Chem. Res.*, 2014, 53, 2299.
- 29 N. J. Wu and X. T. Li, *Polym. Degrad. Stab.* 2014, 105, 265.
- 30 B. B. Wang, Q. B. Tang, N. N. Hong, L. Song, L. Wang, Y. Q. Shi and Y. Hu, *ACS Appl. Mater. & Interfaces* 2011, 3, 3754.

- 31 J. X. Ni, Q. L. Tai, H. D. Lu, Y. Hu and L. Song, *Polym. Adv. Technol.* 2009, 12, 292.
- 32 Z. H. Zheng, J. T. Yan, H. M. Sun, Z. Q. Cheng, W. J. Li, H. Y. Wang and X. J. Cui, *Polym. Int.* 2014, 63, 84.
- 33 Y. Liu and Q. Wang, *Polym. Degrad. Stab.* 2006, 91, 3103.
- 34 Q. Wu, J. P. Lv and B. J. Qu, *Polym. Int.* 2003, 52, 1326.
- 35 K. Wu and Z. Z. Wang, *Polym. Plast. Technol. Eng.* 2008, 47, 247.
- 36 K. Wu, Z. Z. Wang and H. J. M. Liang, *Polym. Compos.* 2008, 29, 854.
- 37 S. Zhang, M. J. Li and N. J. Wu, *Polym. Mater. Sci. & Eng.* 2010, 12, 27.
- 38 J. Zhang, M. J. Bai, Y. Wang and F. Y. Xiao, *Fire Mater.* 2012, 36, 661.

Highlight:

***Colour graphic:** maximum size 8 cm x 4 cm



***Text:** Silicone-microencapsulated aluminum hypophosphite (SiAHP) improved the flame retardancy efficiency but also significantly enhanced the notched impact strength of ABS/SiAHP composites.